IDE∆L®

# High-Field DNP and ENDOR with a Novel Multiple-Frequency Resonance Structure

V. Weis, M. Bennati, M. Rosay, J. A. Bryant, and R. G. Griffin[1]

*MIT/Harvard Center for Magnetic Resonance, Francis Bitter Magnet Laboratory and Department of Chemistry,*
*Massachusetts Institute of Technology, Cambridge, Massachusetts 02139*

We describe a new triply tuned ($e^-$, $^1$H, and $^{13}$C) resonance structure operating at an electron Larmor frequency of 139.5 GHz for dynamic nuclear polarization (DNP) and electron nuclear double-resonance (ENDOR) experiments. In contrast to conventional double-resonance structures, the body of the microwave cavity simultaneously acts as a NMR coil, allowing for increased efficiency of radiofrequency irradiation while maintaining a high quality factor for microwave irradiation. The resonator design is ideal for low-$\gamma$-nuclei ENDOR, where sensitivity is limited by the fact that electron spin relaxation times are on the order of the RF pulse lengths. The performance is demonstrated with $^2$H ENDOR on a standard perdeuterated bis-diphenylene-phenyl-allyl stable radical. In DNP experiments, we show that the use of this resonator, combined with a low microwave power setup (17 mW), leads to significantly higher $^1$H signal enhancement ($\epsilon \sim 400 \pm 50$) than previously achieved at 5-T fields. The results emphasize the importance of optimizing the microwave $B_1$ field by improving either the quality factor of the microwave resonator or the microwave power level.   © 1999 Academic Press

## INTRODUCTION

Electron paramagnetic/nuclear magnetic resonance (EPR/NMR) multiple irradiation techniques are powerful spectroscopic tools for enhancing sensitivity and spectral resolution in conventional NMR and EPR experiments. In a typical dynamic nuclear polarization (DNP) experiment, microwave irradiation is applied to the sample at or close to the electron Larmor frequency in order to transfer polarization from the electron to the nuclear spins. For all polarization mechanisms (*1–6*) the NMR signal enhancement increases with the microwave magnetic field strength. Similarly, in pulsed electron nuclear double resonance (ENDOR) the NMR spectrum is detected by monitoring either the electron spin echo or the electron free induction decay and therefore taking advantage of the high polarization of the electron spins

(*7, 8*). Both double-resonance experiments require high microwave as well as high RF field strengths at the sample position for optimal performance.

In the past decade, the general trend of performing double-resonance experiments (ENDOR and DNP) at increasingly higher fields has led to the implementation of pulse experiments at fields of 3–10 T (*9–14*). Experimental limitations for the implementation of pulse techniques derive from the paucity of high-frequency, high-power microwave ($\mu$W) sources. For DNP experiments at 140 GHz, we have successfully introduced a cyclotron resonance maser (*15*) that provides a high output power of 10–100 W. Nevertheless, routine EPR/ENDOR spectrometers are based on commercially available low-power $\mu$W sources, such as GUNN and IMPATT diodes (<70 mW output power), due to their easy operation, maintenance, and small size. Because of their lower power these sources require high-quality resonator designs in order to achieve reasonable pulse lengths ($t_{\pi/2} < 200$ ns) in pulsed EPR/ENDOR experiments.

Several designs of RF transparent microwave resonance structures for double resonance have been used at X-band EPR frequencies (8–10 GHz) (*16–21*). Initially, slow wave helices were successfully used to increase the microwave magnetic field at the sample position (*16, 17*). In special cases, it was found that helices can lead to higher spin sensitivity than resonant cavities, although the $\mu$W quality factor is reduced by nearly an order of magnitude due to radiation losses of the open structure (*20*). An application of this particular design at high $\mu$W frequencies is not possible for two reasons. First, the resonance frequencies of the helix are fixed by its geometry and do not allow tuning to the microwave frequency of the source. Second, if $2\pi a > \lambda/2$, where $a$ is the radius of the helix and $\lambda$ the free space wavelength of the $\mu$W, the helix no longer acts as a slow wave structure propagating only the fundamental mode. Instead, higher modes and radiative waves are excited without concentrating the electromagnetic energy inside the helix to produce intense microwave magnetic fields (see case (b) in Ref. (*20*)).

[1] To whom correspondence should be addressed. E-mail: griffin@ccnmr.mit.edu.

A more suitable double-resonance design was proposed by Hyde (*18*) and used by Gruber *et al.* (*21*) for X-band frequencies. Based on a cylindrical cavity operating in the $TE_{011}$ mode, the solid metal wall was replaced by a RF transparent helix. Fixed metal top and bottom plates completed the cavity which had a fixed resonance frequency determined by its geometry. Hyde used a one-turn loop consisting of the top and bottom plate of the cavity and additional straps down the side of the cavity completing the loop for RF irradiation. In contrast, Gruber *et al.* employed the windings forming the cavity wall to create the RF field.

In high-frequency ($\geq$90 GHz) EPR and ENDOR, two types of microwave cavity designs are customarily employed: the cylindrical $TE_{011}$ cavity, first proposed by Grinberg *et al.* at 140 GHz (*22*), and the Fabry–Perot resonator (*23, 24*). To date the cylindrical cavity is usually used at frequencies below 200 GHz (*9, 10, 13, 14, 22*), whereas the Fabry–Perot system is currently used above 200 GHz (*25–28*).

The reduced size of the cylindrical resonator operating at a millimeter wavelength does not allow an NMR RF coil to be mounted inside the resonator. An external RF coil, however, suffers from a dramatic loss of RF magnetic field strength at the sample position due to the skin effect (RF skin depth in silver at 211 MHz = 4 $\mu$m). However, for proton ENDOR experiments at 140 GHz (*14*), we recently followed the concept proposed by Burghaus *et al.* at 95 GHz (*9*), which consists of a combination of a high-quality cylindrical cavity with an externally mounted RF coil. In order to allow for RF penetration into the resonator, slots were cut along the cylinder wall, perpendicular to the cavity *z* axis. With this design we were able to achieve a reasonable RF efficiency for proton ENDOR ($\pi$ pulse width of ~13 $\mu$s) by combining a high-quality circuit with moderate RF power ($\leq$400 W). Indeed, pulse lengths on the order of 10 $\mu$s are considered a reasonable compromise between RF power broadening and ENDOR sensitivity. However, the pulse lengths increase with decreasing gyromagnetic ratio of the nuclei. Further, improved efficiency is desirable in ENDOR experiments of low-$\gamma$ nuclei (for instance, $^{13}$C, $^{2}$H, and $^{15}$N) to compensate for effects of short electron spin relaxation times.

Here we describe a new triply tuned ($e^{-}$, $^{1}$H, $X = {}^{13}$C, $^{15}$N, etc.) resonator design based on a helical cylindrical cavity for 140 GHz, which achieves high EPR and NMR conversion efficiencies. We discuss the advantages of employing such a cavity structure in both types of multiple-resonance experiments, DNP and ENDOR. We performed $^{13}$C-detected $^{1}$H DNP experiments on a TEMPO-doped glycerol/water solution, which yield much larger signal enhancements than previously attainable at our field of 5 T. The ENDOR performance is demonstrated with $^{2}$H ENDOR on a standard perdeuterated BDPA stable radical.

## CAVITY DESIGN AND PERFORMANCE

The point of departure for the development of a 140-GHz double-resonance cavity is the standard cylindrical $TE_{011}$ cavity, which combines high $\mu$W conversion efficiency, high filling factor, and a high $Q$ factor (*29*). The motivation arose from the excellent performance recently obtained in pulsed EPR experiments at 140 GHz, where we achieved EPR $\pi$/2 pulse lengths of 60–70 ns corresponding to a microwave magnetic field strength $B_1 \sim$ 1.5–1.25 G at the sample position with 5 mW of incident power. These results were obtained with a cavity radius *r* and length *l* so that $2r/l \sim 1$ and a centered circular iris.

The RF field was introduced into the cavity in a manner similar to that of Gruber *et al.* (*21*), where the cavity wall also serves as the NMR coil. As a result, our new 139.5-GHz EPR resonator is a combination of the $TE_{011}$ cylindrical cavity and an open helical structure. The solid cavity wall is replaced by a flat wound gold-coated copper wire (width, 2.1 mm; thickness, 0.3 mm) forming a five-turn coil with a turn-to-turn distance of 0.1–0.2 mm (Fig. 1a). The total length of the helix amounts to 12.7 mm. As with a slotted cylindrical cavity, the gaps between each coil turn are almost perpendicular to the resonator *z* axis, thereby maintaining the angular electric field distribution of the $TE_{011}$ mode.

At our operating frequency, the performance of the resonator is critically dependent on its mechanical stability, and therefore the helix is inserted into a solid block of Kel-F that also accommodates the leads in appropriate slots (see Figs. 1b and 1c). In this configuration, the position of the helix is fixed inside the housing and with respect to the incident waveguide. Two plungers (Kel-F) with copper end faces (thickness: several $\mu$m) on either side of the coil complete the $\mu$W resonator. The sample is held in place by a fixed plunger, while a movable plunger is used for frequency tuning. The tuned cavity space amounts to one wavelength (~2 mm) and is centered around the iris coupling hole. The plunger end faces are machined to be 0.02 mm smaller in diameter than the plunger itself, thereby preventing electrical shorting of the coil.

The resonator is coupled to a WR-6 (1.65 $\times$ 0.82 mm) waveguide through a circular iris (diameter 0.66 mm), centered in the middle turn of the coil (Fig. 1c). For 140-GHz experiments the use of the WR-6 waveguide with a small cross section prevents the waveguide from shorting several coil turns. Additionally, we observed arcing from the coil to the waveguide during cross polarization and proton decoupling when using a WR-8 waveguide and cooling with helium gas. In the DNP experiments the coil is part of a typical solid-state NMR circuit, which consists of two high-quality *LC* parallel circuits for $^{1}$H ($Q_{1H} = 250$) and low-$\gamma$ nuclei ($Q_{13C} = 110$), respectively, and variable matching and tuning capacitors. The high-voltage variable capacitors are mounted on top of the probe, outside of the cryostat to prevent arcing and tempera-
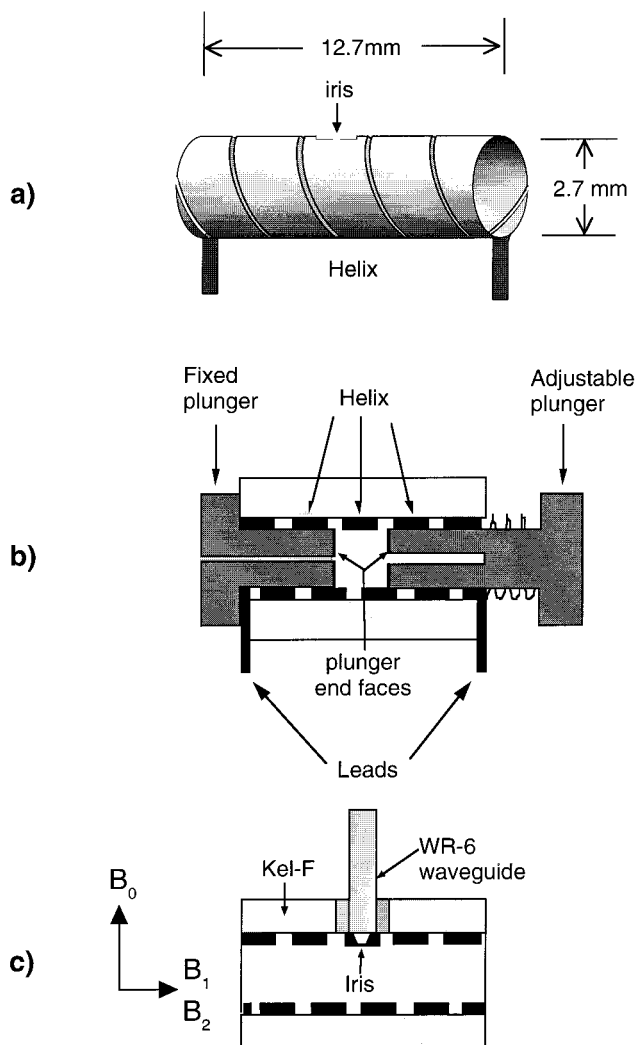
**FIG. 1.** The helix resonator assembly from different views. The helix and both plungers are housed in a Kel-F block to provide mechanical stability and good coupling to the microwave waveguide. The sample is contained in a 0.5- to 0.9-mm-o.d. quartz EPR tube held in place by the fixed plunger. The resonator is tuned to the frequency of the microwave source by moving the adjustable plunger. In the configuration described, the resonator produces microwave $B_1$ and radiofrequency $B_2$ fields parallel with respect to each other and perpendicular to the external Zeeman field $B_0$.

ture-dependent capacitance changes during experiments with helium cooling. A semirigid cable of approximately $\lambda/2$ (for protons) connects the capacitors to the helix.

Microwave pulse lengths were estimated with our custom-designed 139.5-GHz pulsed EPR spectrometer by monitoring the echo-detected EPR signal of an evacuated, standard 1% bis-diphenylene-phenyl-allyl (BDPA) sample as a function of the pulse length. With 5 mW incident power to the cavity we found $\pi/2$ pulse lengths of 80–90 ns, representing an improvement over previously reported values of 100–110 ns obtained with a slotted cylindrical resonator (14). The radiofrequency field strength, $B_2$,

at the sample position was determined with NMR experiments by measuring pulse lengths with conventional methods. Using 0.7-mm-o.d. sample tubes containing 0.3 $\mu$l of doubly $^{13}$C-labeled glycerol we determined both $^1$H and $^{13}$C RF field strengths. Compared to the previously reported double-resonance setup with externally mounted RF coil, we obtained $\pi/2$ pulse widths of 3.8 ($P_{1H}$ = 150 W) and 5 $\mu$s ($P_{13C}$ = 800 W), respectively. Thus, the new helix circuit turns out to be more efficient for $^1$H and $^{13}$C by a factor of ~3.4 and ~2.6, respectively.

## DYNAMIC NUCLEAR POLARIZATION

The performance of the new resonator in DNP was tested with $^{13}$C-detected $^1$H DNP experiments (see Fig. 2) using the solid-state NMR spectrometer mentioned above which employs a 5-T magnet equipped with a $\pm$75-mT superconducting sweep coil (13). A DNP/NMR probe has been built to incorporate a mechanically stable housing for the helical cavity together with a tuning assembly. The microwave source is a GUNN diode with 17 mW output power (Microwave Corp.), connected to the DNP probe via a circulator and an oversized waveguide (WR-42, 0.23 dB/foot attenuation). Before coupling to the resonator, the waveguide is tapered to a WR-6 waveguide (3 dB/foot attenuation). The incident $\mu$W power at the cavity amounts to ~4 mW. Tuning of the resonator is achieved by minimizing the reflected $\mu$W power, monitored through the circulator with a calibrated power meter (HP 432 A).

In order to compare the NMR signal enhancements to previous $^1$H DNP measurements without a cavity (30), a sample of 30 mM 4-amino-TEMPO nitroxide radical in [1,3-$^{13}$C]glycerol/water (60/40) was investigated. The microwave-induced polarization transfer from TEMPO to the $^1$H nuclei was monitored indirectly after cross polarization from $^1$H to $^{13}$C nuclei located in the solvent (see Fig. 2). This allows an accurate
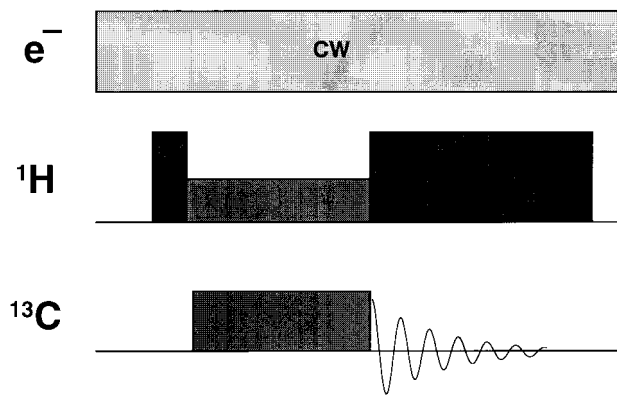


**FIG. 2.** Pulse scheme of the $^{13}$C-detected $^1$H DNP experiment. The microwave is irradiated continuously, driving the polarization transfer to solvent protons. After cross polarization from $^1$H to $^{13}$C, the $^{13}$C free induction decay is detected during $^1$H decoupling.
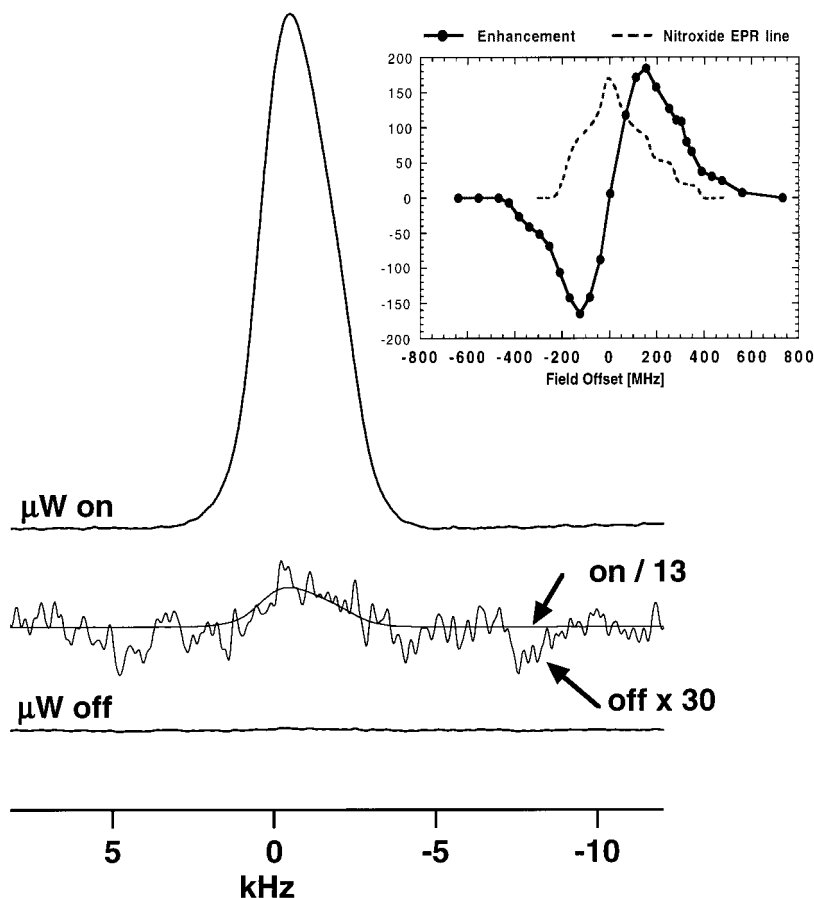
**FIG. 3.** DNP-enhanced $^{13}$C signal of [1,3-$^{13}$C]glycerol/water (60/40) doped with 30 mM 4-amino-TEMPO nitroxide radical. A signal enhancement of $\epsilon \sim$ 400 $\pm$ 50 was observed at $T = 12$ K using the new helical resonator and an incident microwave power of only 17 mW (upper trace). The signal without microwave irradiation is shown in the lower trace. The inset displays the nitroxide EPR line as well as the $^1$H enhancement versus the position of microwave irradiation within the EPR line. The Zeeman field was set to the maximum of the enhancement curve (+150 MHz).

determination of the signal enhancement as no significant $^{13}$C background signal is present.

The sample was loaded into a 0.5-mm-o.d. quartz tube with a filling height of 2 mm to match the dimensions of the resonator ($V \approx 0.25$ $\mu$l). Oxygen was removed on a high vacuum line by performing several freeze, pump, and thaw cycles and flushing with argon gas during sample thawing. The proton $T_1$ relaxation time was measured to be 100 $\pm$ 10 s at $T = 20$ K.

We recently demonstrated (31) that the $^1$H signal enhancement in the TEMPO/water/glycerol matrix occurs via the *thermal mixing effect,* provided that the TEMPO radical concentration is sufficiently high to permit electron–electron spin diffusion across the inhomogeneously broadened EPR line. In that case, energy conserving three-spin flip-flop processes of two electron spins and one $^1$H spin occur at a rate (6)

$$\frac{1}{T_{SSI}} = \frac{1}{T_{2S}} \frac{\overline{|B|^2}}{\omega_I^2} \frac{f(\omega_I)}{f(0)},$$

leading to an enhanced $^1$H polarization. $\omega_I$ is the nuclear Zeeman frequency of the protons, $1/T_{2S}$ is the rate for the above-mentioned simultaneous electron–electron spin flip, and $\overline{|B|^2}$ is a coefficient for the strength of the dipolar coupling between one of the electrons and the protons averaged over all protons in the vicinity of the electron spin. $f(\omega)$ is derived from the normalized EPR lineshape function and indicates the probability of finding two electrons having an energy separation of $\omega$.

The experiment was performed with the magnetic field set to the value for maximum positive signal enhancement (see inset of Fig. 3). Continuous wave microwave irradiation of the sample polarized the solvent protons. Subsequently, cross polarization (CP) to $^{13}$C was performed and the free induction decay (FID) was monitored during proton decoupling (Fig. 2). The RF field strengths were ~60 kHz for a $^1$H $\pi/2$ pulse and 40 and 60 kHz for the CP and decoupling fields, respectively.

Figure 3 compares the cavity-enhanced $^{13}$C signal (upper trace) with the $^{13}$C signal without $\mu$W irradiation (lower trace)

at $T = 12$ K. Both $^{13}$C signals were obtained with an experimental time of 64 min and a recycle delay of 120 s. The observed signal enhancement amounts to $\epsilon \sim 400 \pm 50$ when the resonator is tuned. The uncertainty of the value is primarily due to the extremely small intensity of the unenhanced signal. Previously, maximum enhancements of $\sim 30$ were achieved with the same GUNN diode using a $\mu$W reflector assembly. Larger enhancements could be obtained only when using a high-power $\mu$W source such as our gyrotron (incident power to the probe $\sim 1$–3 W). Enhancements of 185 have been observed under stable gyrotron operation and no microwave cavity.

This improvement of the DNP performance at low levels of $\mu$W power is clearly due to an increase of the $\mu$W magnetic field at the sample position. It also shows that the previously obtained enhancements using high-power microwaves were not limited by the polarizing agent but rather by the efficiency of the $\mu$W irradiation.
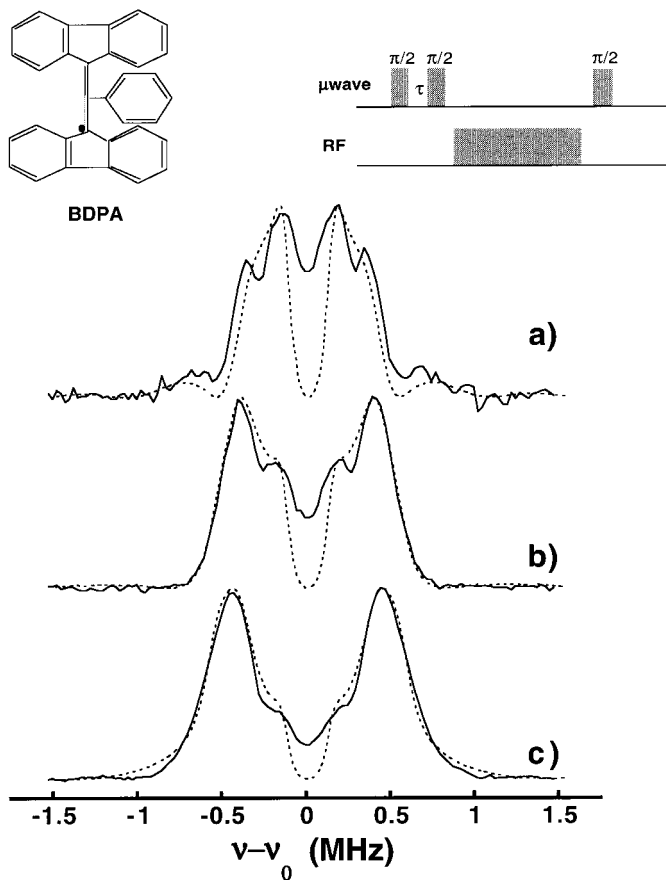
## ENDOR

The ENDOR performance of the double-resonance cavity was demonstrated with $^2$H ENDOR on an evacuated, perdeuterated 0.3% BDPA in a protonated polystyrene matrix. The experiments were performed with a custom-designed 139.5-GHz pulsed ENDOR spectrometer described elsewhere (14).

At 5 T, the Larmor frequencies of low-$\gamma$ nuclei such as $^{13}$C, $^2$H, and $^{15}$N are distributed in a frequency range spanning $\sim 60$ MHz. Thus, a broadband RF circuit that matches this entire frequency range is easier to operate than a high-quality, auto-tunable probe as we use for $^1$H ENDOR. In the following we show that the lower RF efficiency of a broadband circuit still leads to high ENDOR performance when combined with our helical cavity.

The helical cavity was connected in series with a 50-Ohm high-power resistor, resulting in a circuit with the characteristics of a low-pass filter. A 50-Ohm semirigid coax cable with 0.325 in. o.d. and a stranded silver-plated copper inner conductor leads the RF power to the helix. A second semirigid cable connects the helix to the 50-Ohm load, located outside the probe to prevent power heating at helium temperatures. In order to maintain matching and RF efficiency, we use short coil leads of about 10 mm and achieve a coupling of about 10 dB over a frequency range of 0–70 MHz, corresponding to 10% reflected power. Variable incident RF power can be obtained with a pulsed amplifier (American Microwave Technologies Inc., $P_{max} = 2$ kW, 0–130 MHz).

ENDOR spectra were recorded with the Mims-ENDOR technique (32), illustrated in Fig. 4. This sequence is more sensitive to small hyperfine couplings as expected for low-$\gamma$ nuclei than the more popular Davies-ENDOR. In fact, no $^2$H ENDOR spectrum was observed with a Davies-ENDOR sequence. Since the Mims-ENDOR intensity suffers from a periodic dependence on the spacing $\tau$ between the two $\pi/2$



**FIG. 4.** $^2$H Mims-ENDOR spectra of perdeuterated 0.3% BDPA at room temperature. The experimental spectra (solid line) were taken for a pulse spacing $\tau$ of (a) 850 ns, (b) 550 ns, and (c) 250 ns. Other experimental conditions are $t_{\pi/2}$ ($\mu$W) $= 88$ ns, $t_{\pi(RF)} = 85$ $\mu s$, $P_{RF} \sim 400$ W, single scan, and 300 transients/point. The simulation (dashed line) parameters are $g_x = 2.00263$, $g_y = 2.00259$, and $g_z = 2.00234$. The following hyperfine constants are in MHz and represent the absolute values: $^1A_x = 0.25$, $^1A_y = 0.25$, $^1A_z = 0.27$, $^2A_x = 1.18$, $^2A_y = 0.82$, and $^2A_z = 0.3$. (Inset) Structure of BDPA radical.

preparation pulses, given by $I_{ENDOR} \propto 1 - \cos(2\pi A\tau)$, where $A$ is the hyperfine coupling constant, it is desirable to acquire spectra for different $\tau$ values in order to obtain the complete hyperfine information. However, only a limited variation of $\tau$ can be accomplished since the intensity of the electron spin echo decreases substantially due to a fast electronic $T_2$ relaxation time. For our standard, degassed 0.3% perdeuterated BDPA sample, spectra were recorded with pulse spacings between 250 and 850 ns. The samples were loaded into 0.5-mm-o.d. quartz capillaries with a filling volume of about 0.25 $\mu$l.

Figure 4 displays experimental $^2$H ENDOR spectra (solid line) and simulations (dashed line) for the perdeuterated BDPA sample at room temperature. The experimental lineshapes are the result of single RF frequency sweeps, recorded with 300 transients/point and an integration over half the width of the

electron spin echo. Baseline correction was performed by subtracting the spin-echo intensity of two consecutive pulse sequences with and without the RF pulse. The RF pulse length was adjusted on the +0.4-MHz line in order to maximize the ENDOR effect. For about 400 W of power we found a pulse length of ~85 $\mu$s. We note that this value does not correspond to a $\pi$ pulse due to off-resonance contributions in the inhomogeneously broadened ENDOR line, which increase the resulting nutation frequency. Further, with the above optimized RF pulse length and a pulse spacing $\tau = 250$ ns we observed a maximum ENDOR effect of about 30% of the electron spin echo on the +0.4-MHz ENDOR line.

Simulations were performed in order to understand the observed lineshapes. Indeed, a qualitative analysis of Mims-ENDOR spectra, even in a simple example, is very difficult since the spectra are visibly affected by the pulse spacing $\tau$ of the Mims-ENDOR preparation sequence. In perdeuterated BDPA (Fig. 4, inset), the electron spin density is delocalized on the diphenylene rings and alternates between neighboring carbon atoms, resulting in two sets of eight equivalent deuterons. Therefore, two distinguished hyperfine splittings are expected. The hyperfine spectrum was first calculated using two sets of hyperfine couplings and $g$ values which reproduce the EPR spectrum (not shown). We followed the simulation procedure described previously (7) and blindspots were introduced by multiplying the calculated $^2$H spectrum with $(1 - \cos(2\pi*2\nu_{RF}*\tau))*(1 - \langle S_z \rangle)$ (33), where $\tau$ extends from the center of the first microwave pulse to the center of the second. Detailed simulation parameters are given in the figure legend. We note that the simulation satisfactorily reproduces the observed maxima and minima and relative intensities. No evidence for artifacts due to the new experimental setup was observed. The differences observed between experiment and simulation in the depth of the blindspots, particularly at the free Larmor frequency ($\nu - \nu_0 = 0$) for any value of $\tau$, are likely due to fast electron spin diffusion, which is not considered in our simulation. In fact, the discrepancy increases with $\tau$ and is a well-known effect in Mims-ENDOR (34).

## SUMMARY

We have described a new multiple-frequency resonance structure for high-frequency DNP and ENDOR. In DNP experiments, the combination of a high-quality EPR and NMR resonant structure permitted us to achieve a $^1$H signal enhancement of $\sim 400 \pm 50$ with a microwave power of only 17 mW incident on the probe. In conjunction with our existing pulsed EPR board, we are now able to investigate polarization transfer schemes which require pulsed excitation and phase shifts on both microwave and radiofrequency channels. The results are also important since they demonstrate that significantly improved DNP enhancements are possible with an optimized microwave/RF coil.

We also demonstrated the utility of the resonator in ENDOR experiments with $^2$H ENDOR spectra of perdeuterated BDPA. The use of the helical cavity eliminates the problem of the RF penetration through a metallic resonator, which was occurring in the previous high-frequency ENDOR resonators where the RF coil is mounted external on the cavity. The higher RF efficiency, which results in shorter pulse lengths, should facilitate low-$\gamma$-nucleus ENDOR experiments on samples with short electronic relaxation times as well as more sophisticated coherence transfer ENDOR experiments.

## REFERENCES

1. A. W. Overhauser, *Phys. Rev.* **92**, 411 (1953).

2. C. D. Jeffries, *Phys. Rev.* **106**, 164 (1957).

3. A. Abragam, J. Combrisson, and I. Solomon, *C. R. Acad. Sci.* **247**, 2237 (1958).

4. R. A. Wind, M. J. Duijvestijn, C. v. d. Lugt, A. Manenschijn, and J. Vriend, *Prog. NMR Spectrosc.* **17**, 33–67 (1985).

5. M. Goldman, "Spin Temperature and Nuclear Magnetic Resonance in Solids," Oxford Univ. Press, London (1970).

6. W. T. Wenckebach, T. J. B. Swanenburg, and N. J. Poulis, *Phys. Rep.* **14**, 181–255 (1974).

7. A. Grupp and M. Mehring, *in* "Modern Pulsed and CW Electron Spin Resonance" (L. Kevan and M. Bowman, Eds.), p. 195, Wiley, New York (1990).

8. C. Gemperle and A. Schweiger, *Chem. Rev.* **91**, 1481 (1991).

9. O. Burghaus, M. Rohrer, T. Götzinger, M. Plato, and K. Möbius, *Meas. Sci. Technol.* **3**, 765–774 (1992).

10. J. A. J. M. Disselhorst, H. van der Meer, O. G. Poluektov, and J. Schmidt, *J. Magn. Reson.* **116**, 183–188 (1995).

11. T. F. Prisner, *Adv. Magn. Opt. Reson.* **20**, 245 (1997).

12. L. Paschedag, J. van Tol, and P. Wyder, *Rev. Sci. Instrum.* **66**, 5098 (1995).

13. L. R. Becerra, G. J. Gerfen, B. F. Bellew, J. A. Bryant, D. A. Hall, S. J. Inati, R. T. Weber, S. Un, T. F. Prisner, A. E. McDermott, K. W. Fishbein, K. E. Kreischer, R. J. Temkin, D. J. Singel, and R. G. Griffin, *J. Magn. Reson.* **117**, 28–40 (1995).

14. M. Bennati, C. Farrar, J. Bryant, S. Inati, V. Weis, P. Riggs-Gelasco, J. Stubbe, and R. G. Griffin, *J. Magn. Reson.* **138**, 232–243 (1999).

15. L. R. Becerra, G. J. Gerfen, R. J. Temkin, D. J. Singel, and R. G. Griffin, *Phys. Rev. Lett.* **71**, 3561–3564 (1993).

16. K. H. Hausser and F. Reinhold, *Z. Naturforsch. A* **16**, 1114 (1961).

17. R. H. Webb, *Rev. Sci. Instrum.* **33**, 732 (1962).

18. J. S. Hyde, *J. Chem. Phys.* **43**, 1806 (1965).

19. M. R. Pearlman and R. H. Webb, *Rev. Sci. Instrum.* **38**, 1264 (1967).

20. F. Volino, F. Csakvary, and P. Servoz-Gavin, *Rev. Sci. Instrum.* **39**, 1660 (1968).

21. K. Gruber, J. Forrer, A. Schweiger, and H. H. Gunthard, *J. Phys. E: Sci. Instrum.* **7**, 569 (1973).

*22.* O. Grinberg, A. A. Doubinskii, and Y. S. Lebedev, *Russ. Chem. Rev.* **52,** 850 (1983).

*23.* I. Amity, *Rev. Sci. Instrum.* **41,** 1492 (1970).

*24.* E. Haindl and K. Möbius, *Z. Naturforsch. A* **40,** 169 (1985).

*25.* D. E. Budil, K. A. Earle, W. B. Lynch, and J. H. Freed, *in* "Advanced EPR: Applications in Biology and Biochemistry" (A. J. Hoff, Ed.), pp. 307–340, Elsevier, Amsterdam (1989).

*26.* C. Kutter, H. P. Moll, J. van Tol, H. Zuckermann, J. C. Maan, and P. Wyder, *Phys. Rev. Lett.* **74,** 2925 (1995).

*27.* G. M. Smith, J. C. G. Lesurf, R. H. Mitchell, and P. C. Riedi, *Rev. Sci. Instrum.* **69,** 1 (1998).

*28.* M. Fuchs, S. Weber, K. Möbius, M. Rohrer, and T. Prisner, International Experts Workshop of HF-EPR Instrumentation, Urbana–Champaign (1998).

*29.* C. P. Poole, "Electron Spin Resonance," Wiley, New York (1983).

*30.* D. A. Hall, D. A. Maus, G. J. Gerfen, S. J. Inati, L. R. Beccera, F. W. Dahlquist, and R. G. Griffin, *Science* **276,** 930–932 (1997).

*31.* D. A. Hall, S. J. Inati, C. T. Farrar, G. J. Gerfen, and R. G. Griffin, manuscript in preparation (1998).

*32.* W. B. Mims, *Proc. R. Soc. A* **283,** 452–457 (1965).

*33.* P. Höfer, Ph.D. thesis, University of Stuttgart (1988).

*34.* W. W. Mims, K. Nassau, and J. D. McGee, *Phys. Rev.* **123,** 2059 (1961).